USA-JAPAN WORKSHOP

ON SUBMILLIMETER DIAGNOSTIC TECHNIQUES

January 18-21, 1982

Nagoya, Japan

FAR-INFRARED IMAGING ARRAYS FOR FUSION PLASMA DENSITY AND MAGNETIC FIELD MEASUREMENTS

D.P. Neikirk and D.B. Rutledge

Division of Engineering and Applied Science

California Institute of Technology

Pasadena, CA 91129

H. Park, N.C. Luhmann, Jr., W.A. Peebles and C.X. Yu

Department of Electrical Engineering

University of California, Los Angeles, CA 90024

Far-infrared imaging detector arrays are required for the determination of density and local magnetic field in fusion plasmas. Analytic calculations point out the difficulties with simple printed slot and dipole antennas on ungrounded substrates for use in submillimeter wave imaging arrays because of trapped surface waves. This is followed by a discussion of the use of substrate-lens coupling to eliminate the associated trapped surface modes responsible for their poor performance. This integrates well with a modified bow-tie antenna and permits diffraction-limited imaging. Arrays using bismuth microbolometers have been successfully fabricated and tested at 1222μm and 119μm. A 100 channel pilot experiment designed for the UCLA Microtor tokamak is described.

I. INTRODUCTION

Laser interferometry is used to measure the spatial and temporal behavior of the electron density of high density plasmas such as those which are produced in tokamaks. The electron density is determined indirectly from a measurement of the dielectric constant which is density dependent. Both Mach-Zehnder and Michelson type interferometers have been used to measure the phase shift, and hence, the electron density. The phase difference ϕ between the two arms caused by the plasma of thickness L in one of the interferometer legs is given by

$$\phi = k_o L - \int_o^L k_p(\ell)d\ell = \frac{\omega_o L}{C}\left\{1 - \frac{1}{L}\int_o^L \left(1 - \frac{n_e(\ell)}{n_c}\right)^{\frac{1}{2}} d\ell\right\}$$

where ω_o is the probe frequency and n_c is the critical density. To avoid refraction problems and plasma resonances one operates with $\omega_o >> \omega_{pe}$. Under these conditions, the expression for the phase shift simplifies considerably to

$$\phi \simeq \frac{\pi}{\lambda_o n_c}\int_o^L n_e(\ell)d\ell = \frac{\pi L}{\lambda_o}\frac{n_e}{n_c}$$

assuming a constant density plasma. To obtain several fringe shifts in the current generation of devices ($L \simeq 1m$, $10^{13} < n_e < 10^{14} cm^{-3}$), requires a far-infrared laser. The short wavelength (minimum fringe shift) limit is imposed by mechanical vibrations of the interferometer which can lead to spurious phase shifts.

This interferometer measures only a single chord-averaged density, and it would be desirable to probe the plasma along multiple chords using a multichannel interferometer. Then with the appropriate symmetry assumptions (or a tomographic scan), the radial density profile can be obtained by unfolding the spatial density profile.

The first FIR multichannel system was an 8-channel system developed by Vernon and his collegues for the French TFR tokamak.[1] This employed an HCN electric discharge laser together with a rotating grating to provide the required frequency modulation at the operating wavelength of 337μm. A second type of dual-beam modulated system introduced by Wolfe and his co-workers[2] utilizes twin optically-pumped far-infrared lasers which are offset from each other in frequency by about 1 MHz. Operating at λ = 118.8 μm with output power of 40 mW from each of the CH_3OH lasers has allowed five channel operation on Alcator C.[3] The system is capable of determining, with Abel inversion techniques, the evolution of the density profile in time. The sensitivity is 10^{-1} fringes and is limited by vibrations to a minimum detectable density of 2×10^{12} cm^{-3}.

To overcome the problem associated with mechanical vibrations, a common path HeNe interferometer has been used in conjunction with a dual-beam interferometer at λ = 118.8 μm on PDX.[4] Because the phase shift due to the plasma scales as wavelength λ, the contribution of the plasma in the HeNe (0.633 μm) measurements can be neglected. Hence, the HeNe beam measures only the vibration contribution which can be used to correct the far-infrared measurements. As an example of the results, a system is under construction for use on TFTR to provide 10 channels and will require 400 mW of laser power at λ = 118.8 μm. A similar system has been operated on JIPP-TII with HeNe vibration compensation and 10 mW of power in two channels from twin CH_3OH lasers.[5] Sensitivity of 1/40 fringe which corresponds to a minimum detectable density of 8×10^{11} cm^{-3} has been achieved.

Although the above mentioned systems represent impressive technological achievements, one actually desires significantly greater numbers of channels in order to accurately determine density profiles even in plasmas possessing a relatively high degree of symmetry. Unfortunately, the discrete channel and detector technology employed in the present systems does not lend itself well to significant increases

in channel number. Specifically, the economic costs as well as the increased complexity are prohibitive. As will be discussed in more detail later, the development of an integrated imaging FIR detector array will alleviate these difficulties.

The determination of the plasma magnetic field is also of great importance for magnetic fusion confinement. For example, a knowledge of the poloidal magnetic field distribution is essential in understanding tokamak confinement. A typical technique is to employ Faraday rotation to ascertain the magnitude of the local magnetic field. For $\omega >> \omega_{pe}, \omega_{ce}$ the rotation angle ϕ is given by

$$\phi \alpha \lambda_o^2 \int_o^L n_e(\ell)\, B_o(\ell) d\ell \quad .$$

The λ_o^2 dependence results in a choice of a far-infrared system for typical tokamak parameters. A second point to note is that this measurement only provides the chord-averaged product of density and magnetic field. One again requires an imaging array to accurately unfold the desired plasma parameters.

Finally, one should note that there is also considerable interest in the study of spontaneously occurring low frequency ($\leq$ MHz) microturbulence in tokamaks. Such low frequency fluctuations are of interest since they may be responsible for the anomalously large electron heat conduction observed in tokamaks. As discussed in a companion paper in this workshop, we have performed the first FIR scattering measurements of low frequency electostatic fluctuations in the drift wave and convective cell frequency range using conventional discrete single channel detectors. The advantages of a detector array in these studies are obvious. Much less work has been done in studying magnetic fluctuations in tokamaks. These have been restricted to probe studies in rather low energy density tokamaks.[6-10] However, these probe studies have shown a broadband spectrum of magnetic fluctuations at frequencies up to several hundred kilohertz.

Amplitudes as large as $\tilde{B}_r/B_T \simeq 10^{-4}$ have been measured although no definite connection with density fluctuations or anomalous transport has been established.[10] Faraday rotation measurements with an imaging detector array with MHz frequency response offer the potential of localized nonperturbing $\tilde{B}$ measurements in fusion temperature plasmas.

With the goal of addressing the abovementioned diagnostic needs, a collaborative imaging array program was established at Cal Tech and UCLA. The specific purpose has been the development of a sensitive room temperature imaging array in the 100 - 1000μm region. As will be shown below, this required first the solution of the antenna coupling problem in order that high efficiency could be achieved with minimum "crosstalk" between antenna elements. In addition, a sensitive integrated detector element with moderate speed and high fabrication yield was also required. Both of these constraints have been satisfied and arrays at 119μm and 1222μm have been fabricated and tested. A 100 channel pilot interferometer experiment for the UCLA Microtor tokamak is currently under preparation.

The organization of this paper is as follows. Section II contains background information on imaging arrays. The problem of surface wave coupling in the case of dipoles and short slots on substrates is addressed in Section III. The use of substrate-lens coupling to eliminate these undesirable modes is described in Section IV together with the performance at 119μm and 1222μm of a bow-tie antenna system with bismuth microbolometer detectors fed by such an arrangement. Finally, details concerning the 100 channel Microtor interferometer system currently under development are contained in Section V.

The basic idea of an imaging antenna array is shown in Fig. 1. A lens focuses an image on an array of antennas with individual detectors. Where the intensity is greatest, the detectors receive the most power. An image is obtained by plotting the signal received by each antenna. This is different from a conventional phased array in which the outputs of the antenna are combined. In this array, each antenna has its own detector. One possible design for this array is a group of resonant microstrip dipoles like those used at centimeter wavelengths.[19] However, the losses of microstrip antennas increase greatly at high frequencies. Microstrip substrates must be much thinner than a wavelength. This makes them difficult to make at short wavelengths.

Another approach is to put a resonant dipole[20] or slot[15] on a substrate. Typically, radiation is coupled in from the back side and the substrate is made thin, ~ $\lambda_0/10$. One aspect that must be considered in these antennas is the effect of surface waves. We can understand how the surface waves are excited by considering Figure 2. In the figure, a transmitting antenna lies on a substrate. From a ray point of view, the energy that radiates into the substrate at angles larger than the critical angle is completely reflected and trapped as a surface wave. This power is then lost or captured by other antennas. This surface-wave crosstalk decays slowly; the power falls off only as 1/r. The power is difficult to calculate, but recently Uzunoglu et al. have made excellent progress in calculating the properties of microstrip dipoles.[19] They found that a resonant dipole on a substrate with a dielectric constant of 9.9 and a thickness of $0.21\lambda_d$ lost 2/3 of its power to surface waves.

II. IMAGING ARRAYS

Imaging at far-infrared and millimeter wavelengths is usually done by a single detector with scanned optics.[11,12] However, this mechanical scanning is too slow for many plasma imaging applications where microsecond response times are required. Here a multichannel array of detectors is needed rather than a single scanned detector. Several researchers have pointed out that this would be particularly attractive as a monolithic integrated circuit.[13,14,15]

There are several potential choices for a monolithic far-infrared imaging array. Pyroelectric vidicons have been successful at shorter wavelengths[16] and are quite sensitive at low chopping speeds. However, they are much less sensitive at MHz frequencies. Another alternative is an array of monolithic Schottky diodes like those developed by Clifton.[15,17] These are sensitive and fast, and are an attractive approach at millimeter wavelengths when they can be successfully made in arrays. They have not been demonstrated at 119μm, the prime plasma diagnostic wavelength. A third detector is the bismuth microbolometer developed by Hwang and Schwarz.[18] This device is easy to fabricate and is moderately sensitive, with an NEP of $10^{-10} W/\sqrt{Hz}$ at a modulation frequency of 1MHz. These work throughout the far-infrared and should be useful where extreme sensitivity and speed are not needed.

Given the progress in planar detectors, it is crucial to develop designs for imaging arrays. We have developed a monolithic imaging antenna array at a wavelength of 1.2mm. There are two significant advances: the optical system and the antenna design. Radiation is coupled in by a lens placed on the back of the substrate. The antenna is a modified bow tie. The system provides diffraction-limited imaging at 1.2 mm. We have also fabricated an array for a wavelength of 119 μm and have made preliminary tests.

III. SURFACE WAVES

We can get a feeling for the way surface waves are excited by considering a simpler case. The field for a dipole and a short slot on a substrate can be found in closed form. This can be done as the solution to a boundary value problem, but it is easiest to calculate by reciprocity.[21] The radiated fields of a dipole or a slot on a substrate differ from the fields of a dipole or slot in free space by the ratio of the incident and transmitted fields for plane waves. The surface waves can also be calculated from reciprocity.[22] It can be shown that the power radiated by the slot into a surface mode can be written in the form

$$P = \begin{cases} \dfrac{3\varepsilon_r \lambda_o}{16\, h_e} & \text{for TM modes} \\ \dfrac{3\varepsilon_r \lambda_o \cos^2\theta}{16\, h_e} & \text{for TE modes} \end{cases}$$

where P is the power normalized to the power the slot would radiate in a vacuum, h_e is the effective height of the mode defined by Kogelnik[23], and θ is the angle of incidence within the substrate. (See Pg. 27 in Ref. 23).

The formula for dipoles is similar:

$$P = \begin{cases} \dfrac{3\lambda_o \cos^2\phi}{4\, h_e} & \text{for TE modes} \\ \dfrac{3\lambda_o \sin^2\phi \cos^2\theta}{4\, h_e} & \text{for TM modes} \end{cases}$$

where P is the power normalized to the power the dipole would radiate in vacuum and ϕ is the phase shift[23] of the wave when it reflects from the surface. These formulas mean that if the effective height of the mode is small, that is, if the actual guide height is small and the mode is tightly bound, then the surface mode will be strongly excited.

The power radiated and the power lost to surface modes can be calculated from these formulas on a programmable calculator. Figure 3 shows the calculated power distribution for a short dipole on a substrate with a dielectric constant of 12. This is appropriate for silicon and gallium arsenide substrates. It is clear that unless the substrate is extremely thin, most of the power is lost to surface waves. This is because the dipole is strongly coupled to the TE_o surface mode, even in thin substrates. Figure 4 shows the power distribution for a short slot. Again, unless the substrate is thin, most of the power is lost to surface waves. Note that a slot on this substrate radiates 20 times more power than a slot in free space. Figure 5 shows how these surface wave losses affect the gain. The dipole gain is greatly reduced even for thin substrates. The slot gain is also reduced when the substrate is thicker than $\lambda_o/20$. At far-infrared wavelengths thicknesses required for dipoles are probably too thin to be practical. It will cause some difficulty for slots as well; the required thickness at 119μm is about 6 μm. This maybe practical for single devices but it may be difficult for large arrays.

These graphs suggest another approach. The problem is that the antennas radiate preferentially into the substrate. Most of the energy is beyond the critical angle and is trapped as surface waves. If we curve the back side of the substrate to form a lens, the rays will be incident at a small angle, so that the rays are not trapped.

IV. SUBSTRATE-LENS COUPLING

Figure 6 shows the idea in which imaging is done through the substrate and a substrate lens of the same material. The system is similar to an oil-immersion microscope, except that the positions of the object and the image are reversed. This substrate-lens coupling has several advantages. The trapped surface waves are eliminated because waves transmitted from the antennas are incident at a small angle on the lens surface. Power is coupled in from the substrate where the antenna is most sensitive. In microwave tests on large scale models, we found that 50% of the power focused by the objective lens is coupled into the array. Another advantage is that the optical system can be made nearly aplanatic, with virtually no spherical aberration or coma.[24] Finally, this approach integrates well with the modified bow-tie antenna, allowing us to approach diffraction-limited imaging. The disadvantages are those of any optical system with lenses: material and reflection loss. These can be reduced to a minimum by using low loss materials and quarter-wave matching layers on the lens surfaces.

The antenna array design is shown in Fig 7. The antenna spacing is a compromise that gives adequate sampling, coupling efficiency, and antenna patterns. The antenna is a modified bow tie. One unusual feature of this antenna is that the low-frequency leads are formed by extending the arms of the bow. We found in microwaves tests that crosstalk between adjacent antennas is low, 19dB down for antennas half a dielectric wavelength apart. The bow angle of 60° gives an impedance of 150Ω to match to the bismuth microbolometers. Reference (21) gives the design details. Figure 8 is a photomicrograph of an array for 1.2mm. The substrate is fused quartz. The antennas are evaporated silver 75nm thick with a spacing of 310 μm. The narrow

lines are evaporated bismuth, also 75nm thick. All patterns are formed by contact photolithography and lift-off. The DC resistances of the bolometers lay in the range 100-150Ω. Figure 9 shows the substrate lens mounted on the array.

The far-infrared measurements were made at 1.22mm using a CO_2-pumped $C^{13}H_3F$ laser with a power output of 3mW. The TPX objective lens had a 70-mm focal length and a 50-mm diameter. The fused-quartz substrate lens had a 6.62-mm radius. The thickness of the lens-substrate combination was 10mm. To provide a point source, we focused the laser beam with another TPX lens to a spot a few millimeters in diameter at a distance of 1.4m from the imaging system. When focused on this spot, the optical system had a magnification of 3.2^{o} in the far field per millimeter in the image plane. This corresponds to 1.0^{o} per antenna. Reference (25) gives more experimental details.

We tested the resolution of the array with a pair of pinholes illuminated by a laser. Our pinholes were 5-mm holes drilled in a copper plate, spaced to give a point-source separation 20% larger than the Rayleigh limit. A stack of fused-quartz cover slips delayed one beam so that the two sources were in phase quadrature. The intensity distribution is identical to that of two incoherent point sources.[26] Figure 10 shows that the array resolves them easily.

The measured responsivity of the array elements was 1-2V/W at the relatively low bias of 1 mA. Previous measurements[27] have shown that the bolometers are 1/f noise limited up to 100 kHz and that they have a frequency response of 5 MHz. We expect the array to have a Johnson-noise limited NEP from 100 kHz to 5 MHz of 10^{-9} $W/\sqrt{Hz}$. As will be shown below, this sensitivity and speed should be adequate for far-infrared plasma interferometer measurements. Work is under way to determine the losses and coupling efficiencies. The field of view of the array, 8 antennas, is presently limited by the size of the substrate

lens. We have also fabricated an array for 119μm. Fused quartz is lossy at this wavelength, so the substrate and lens are made of silicon. Preliminary tests indicate that this array is as sensitive as the 1.2-mm array.

V. 100 CHANNEL MICROTOR INTERFEROMETER

As mentioned earlier, a 100 channel pilot interferometer experiment is being prepared for the UCLA Microtor tokamak. If this is successful it will later be configured as a polarimeter for the simultaneous measurement of $\int n_e d\ell$ and $\int n_e B d\ell$ with the same probe beam as originally done by Dodel and Kunz for a single channel.[28]

It is appropriate at this point to estimate the signal-to-noise ratio that will result using the present detector arrays together with commonly available CW FIR sources. As shown in Table 1, a power level of ≈ 100mW is obtainable throughout most of the FIR. To calculate the amount of power falling on each detector we must consider the actual optical system. For purposes of calculation, we will restrict our attention to the UCLA Microtor tokamak which will be used for the first pilot experiment. As in our present FIR scattering studies, the beam will enter vertically through a roughly pie-shaped port. Here, the port will be approximated as a rectangle with a 2.5 cm x 20 cm clear aperture.

The simplest optical system would utilize a cylindrical probe beam with a diameter of ≈ 20 cm. However, this is extremely wasteful and results in an effective area of only ≈ 16%. As we shall see, this results in an unacceptable degradation in signal level. Therefore, our system design is based on the assumption of rectangular probe beam with dimensions comparable to the tokamak part dimensions.

The optical system losses are dependent on the choice of operating frequency. At wavelengths of ≈ 0.8 - 1.2mm, teflon windows and lenses may be employed with little loss. Overall efficiencies as high as 50% are easily realizable. For the shorter wavelengths, absorption in lenses and windows can be significant. To reduce these losses, single crystal quartz windows and reflective optics are

commonly employed at the shorter wavelengths ($\lambda_o < 300\mu m$). For estimation purposes we have assumed an overall loss factor of 3dB at the longer wavelengths and 6dB at the shorter wavelengths. The former number is well known from our FIR laser scattering experience. The latter number may be too pessimistic and may be revised downward as we gain experience at the shorter wavelengths.

For the initial measurements of the time development of the plasma density and poloidal field distribution, a bandwidth of ≃ 50 kHz will be sufficient. The detector array will provide 100 data channels. Assuming a probe input power level of ≃ 100 mW this results in an effective power per detector of ≃ 500μW and ≃ 250 μW for long and short wavelength operation, respectively. This implies a minimum signal-to-noise ratio of ≃ 30dB. This suggests that even with only ≃ mW input power the measurement will be possible. Note that had we simply utilized a 20 cm diameter cylindrical input beam the calculated signal-noise level would have been reduced to ≃ 10^2 even at the higher power level. As a final note, we should point out that even with a bandwidth of several MHz the measurements appear feasible. This will permit the study of both density and magnetic field fluctuations.

As mentioned earlier, the measured responsivity of the detector elements is ≃ 1-2 V/W. We therefore anticipate an output voltage of ≃ 50-500 μV from each channel. The signals will be digitized in LeCroy Model No. 2264 Waveform Digitizers which have a 100kHz sampling rate when operated in the eight channel mode. Using the bipolar input, the signal input range is ± 256mV. We therefore require a voltage amplification of ≃ 3 x 10^3 or ≃ 70dB. To provide a margin for source and detector variations a maximum amplifier gain of 90dB was selected. Let us now calculate the required amplifier noise figure. The microbolometer can be modeled as an open circuit voltage source (≃ 1V/W) in series, with a 100Ω resistor.

Assuming an amplifier input impedance of 50Ω, an incident power of 100μW per detector, a bandwidth of 50 kHz, and requiring a signal-noise ration of 30dB results in a required IF noise temperature of less than 3×10^4 °K. Therefore, even for bandwidths as high as several MHz such large S/N ratios can be maintained with readily available commercial low frequency amplifiers with noise figures of 1-2dB. The only serious amplifier constraint is therefore the cost per channel. We are presently investigating various alternatives in order to keep the cost per channel below ≈ $200.

VI. SUMMARY

Substrate-lens coupling has been shown to eliminate trapped surface modes. This approach has been used with modified bow-tie antennas and bismuth microbolometers to produce the first sensitive imaging arrays in the 100 - 1000μm region. A pilot interferometer experiment using these arrays is being developed for the UCLA tokamak.

Acknowledgements

This work was supported by U.S. DOE-OMFE Contract DE-AM03-76SF00010.

References

1. Veron, D., Certain, J., and Crenn, J.P., J. Opt. Soc. Am., 67, 964-967 (1977).
2. Wolfe, S.M., Button, K.J., Waldman, J., and Cohn, D.R., Appl. Opt., 15, 2645-2648, (1976).
3. Wolfe, S.M., Proceedings of the Japan - USA Workshop on Far-Infrared Plasma Diagnostics, Cambridge, Mass., January 27-29, (1980).
4. Mansfield, D.K., Johnson, L.C., and Mendelsohn, A., Int'l J. IR and Millimeter Waves, 1, 631-640, (1980).
5. Nishizawa, A., Noda, N., Yamanaka, M., Takeda, Y., Okajima, S., Makino, S., Nagasaka, K., Koizumi, T., Yabusaki, H., Takai, M., Murakami, Y., Nagashima, A., Tsunawaki, Y., and Fujita, J., in Digest of the 5th Int. Conf. on Infrared and Millimeter Waves, Wurzburg, W. Germany, October 6-10, (1980).
6. Zweben, S.J., Menyuk, C.R., Taylor, R.J. Phys. Rev. Lett. 42 1270 (1979).
7. Kubena, R.L., Ph.D. Thesis, California Institute of Technology, Pasadena (1978).
8. Hedemann, M., Ph.D. Thesis, California Institute of Technology, Pasadena (1981).
9. Taylor, R.J., Gould, R.W., Hedemann, M.A., Lee, P., Levine, B.S., Luhmann, N.C., Jr., Mase, A., Morales, G.J., Peebles, W.A., Semet, A., Schwirzke, F., Talmadge, S., Zweben, S.J., Plasma Physics and Controlled Nuclear Fusion Research Proc. 8th Int. Conf., Brussels, (1980).
10. Zweben, S.S. and R.J. Taylor, Nucl. Fus. 21, 193 (1981).
11. Hodges, D.T., Foote, F.B., Reber, E.E. and Schellenbaum, R.L.,"Near Millimeter Wave Radiometric Imaging," Conference Digest, Fourth Int. Conf. on Infrared and Millimeter Waves and Their Applications, IEEE Cat. No. 79 CH 1384-7 MTT, pp. 51-52, (1979).
12. Waldman, J., Fetterman, H.R., Duffy, P.E., Bryant, T.G., Tannenwald, P.E., "Submillimeter model measurements and their applications to millimeter radar systems," Fourth Int. Conf. on Infrared and Millimeter Waves and Their Applications, IEEE Cat. No. 79 CH 1384-7 MTT, pp. 49-50, (1979).

13. Luhmann, N.C., Jr., "Instrumentation and Techniques for Plasma Diagnostics: An Overview," in Infrared and Millimeter Waves, Vol. 2, K.J. Button, ed., Academic Press, New York, p. 1-65, (1979).

14. Gordon, G.A., Hartman, R.L., Kruse, P.W., "Imaging-Mode Operation of Active NMMW Systems," Infrared and Millimeter Waves, Vol. 4, K.J. Button, ed., Academic Press, New York, p. 327-352, (1981).

15. Clifton, B.J., Murphy, R.A., Alley, G.D., "Integrated monolithic mixers on GaAs for Millimeter and submillimeter wave applications," Conference Digest, Fourth International Conference on Infrared and Millimeter Waves and Their Applications IEEE Cat. No. 79 CH 1384-7, MTT, p. 84-86, (1979).

16. Hindin, H., "Pyroelectric array images by night," Electronics, p. 47-48, June 16, 1981.

17. Clifton, B.J., Alley, G.D., Murphy, R.A., Mroczkowski, I.H., "High-performance quasi-optical GaAs monolithic mixer at 110 GHz," IEEE Trans. Electron Dev., ED-28, pp. 155-157, (1981).

18. Hwang, T.L., Schwarz, S.E., Rutledge, D.B., "Microbolometers for Infrared Detection," Appl. Phys. Lett., 34, pp. 773-776, (1979).

19. Uzunoglu, N.K., Alexopoulos, N.G., Fikioris, J.G., "Radiation Properties of Microstrip Dipoles," IEEE Trans Antennas and Propagat., AP-27, pp. 853-858, (1979).

20. Mizuno, K., Daiku, Y., Ono, S., "Design of Printed Resonant Antennas for Monolithic Detectors," IEEE Trans Microwave Theory Tech., MTT-25, pp. 470-472, (1977).

21. Rutledge, D.B., Muha, M.S., Imaging Antenna Arrays, to be published, IEEE Trans. Antennas Propagat.

22. Rutledge, D.B., unpublished.

23. Kogelnik, H., "Theory of Dielectric Wavequides," Integrated Optics, Tamir, ed., Springer-Verlag, New York, (1975).

24. Jenkins, F.A., White, H.E., Fundamentals of Optics, Fourth Edition, McGraw-Hill, N.Y. pp. 166-170, (1976).

25. Neikirk, D.P., Rutledge, D.B., Muha, M.S., Park, H., Yu, C.X., "Far-infrared imaging antenna arrays," to be published, Appl. Phys. Lett.

26. Goodman, J.W., Introduction to Fourier Optics, McGraw-Hill, N.Y. (1968).

27. Rutledge, D.B., Schwarz, S.E.,"Planar multimode detector arrays for infrared and millimeter-wave applications,"IEEE J. Quantum Electron, QE-17, 407, (1981).

28. Dodel, G. and Kunz, W., Infrared Phys. 18, 773, (1978).

Table 1. Power Output of Commonly Available CW FIR Sources.

Source	λ_o (μm)	P_o (mW)
Laser	1222	7
Carcinotron	1000	300
Carcinotron	800	80
Laser	447	30
Laser	185	100
Laser	119	100

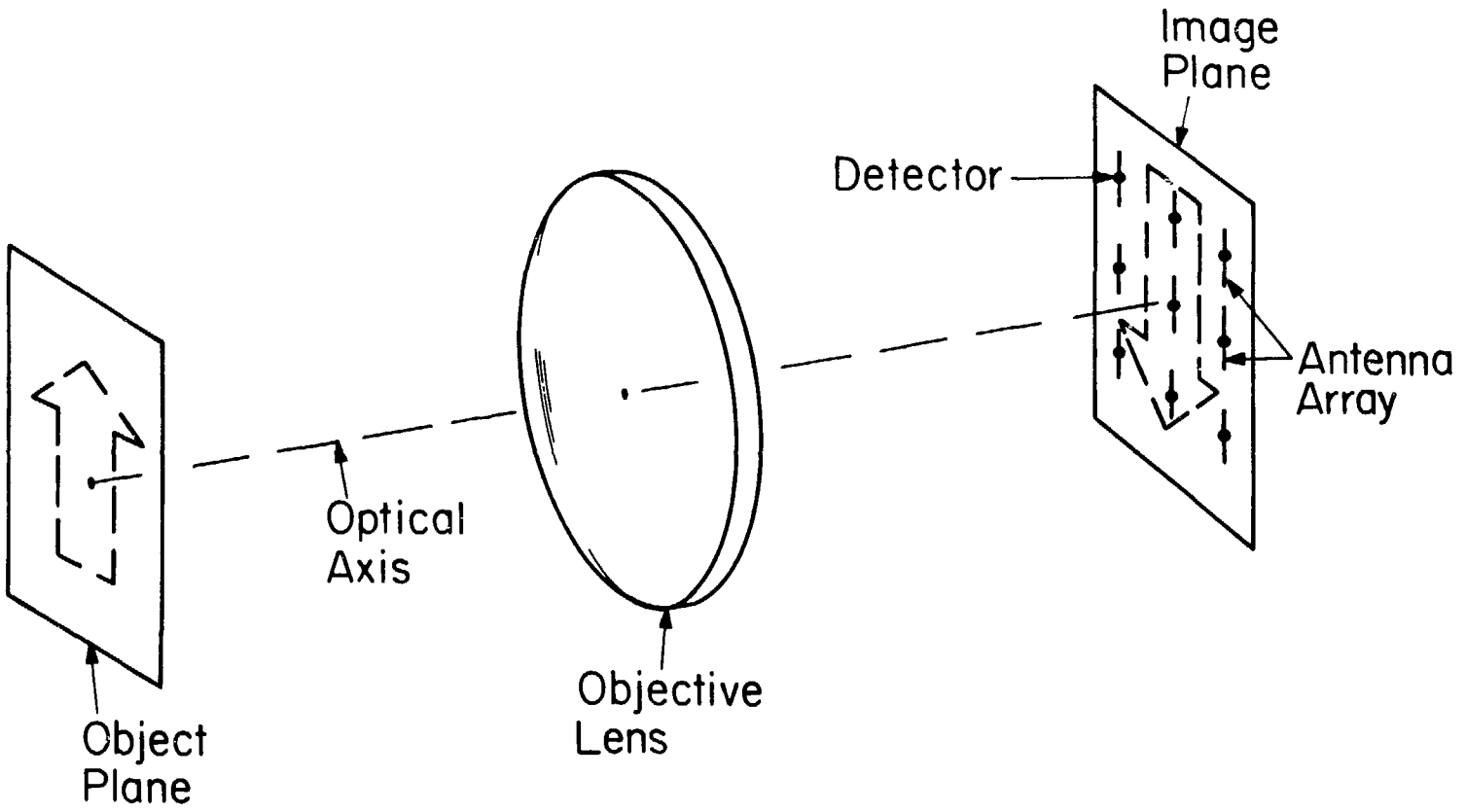

Fig. 1 Imaging with an array of antennas with individual detectors at the image plane.

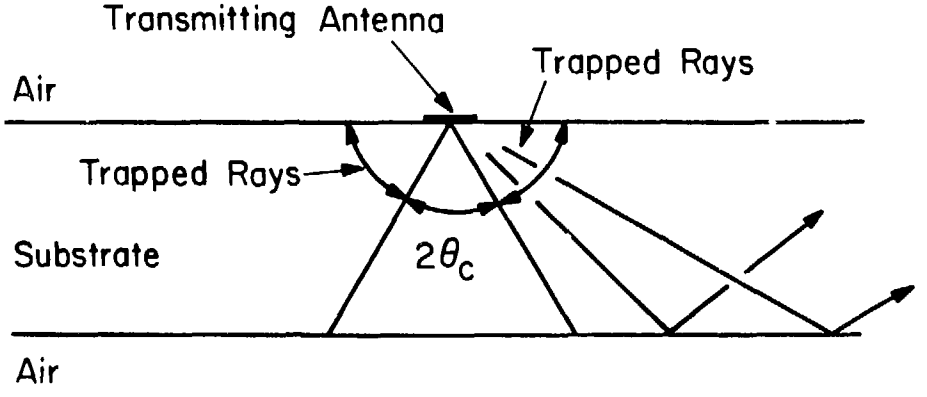

Fig. 2 Ray picture of excitation of trapped surface waves on a substrate. Substrate rays outside the wedge $2\theta_c$ are completely reflected and trapped as surface waves. The critical angle (30^o) shown is appropriate for fused quartz ($\varepsilon_r = 4$).

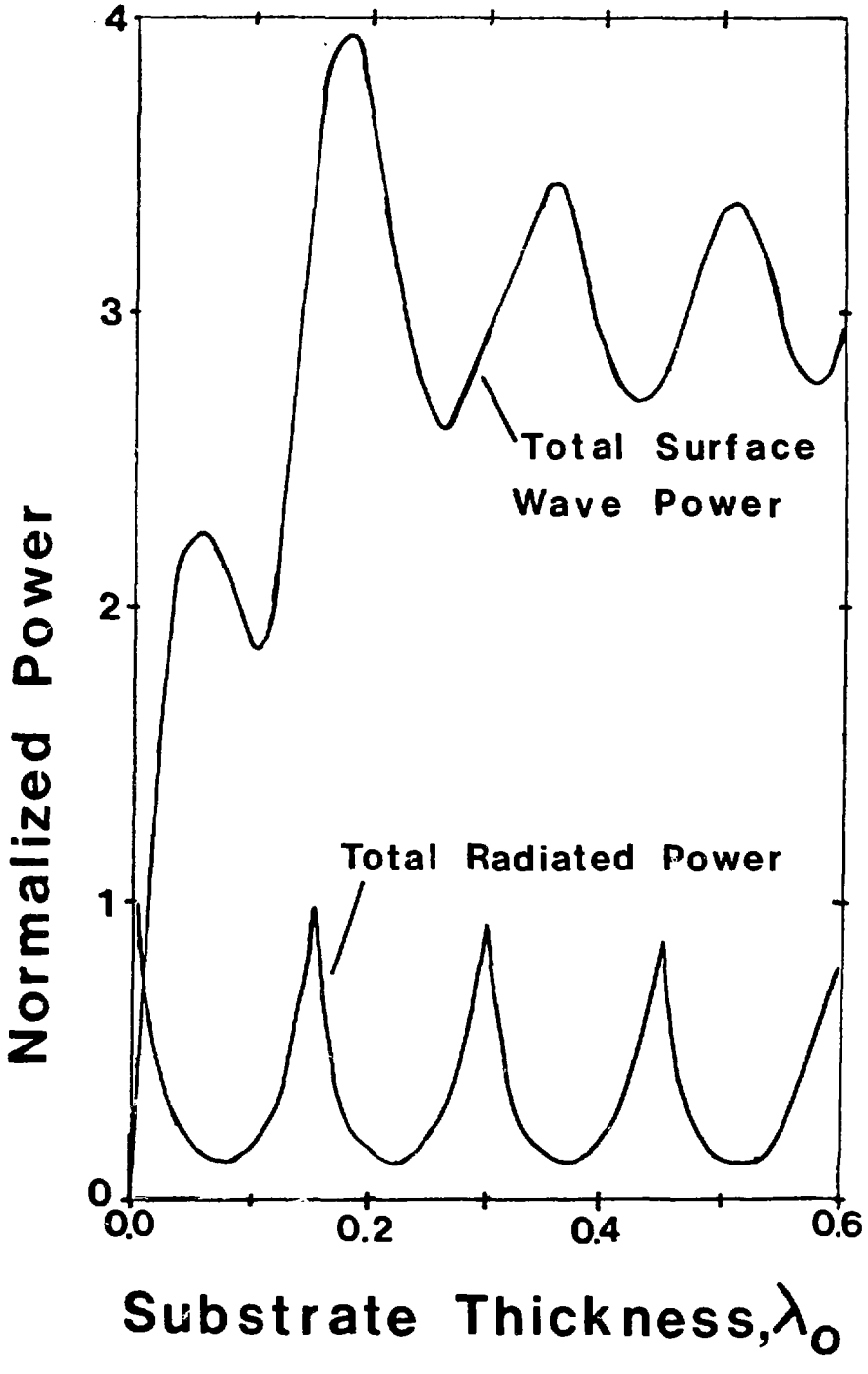

Fig. 3 Calculated distribution of power radiated by a short dipole on a substrate with a dielectric constant of 12. Power is normalized to the power the same dipole would radiate in free space. Surface waves dominate for thicknesses greater than $\lambda_o/100$.

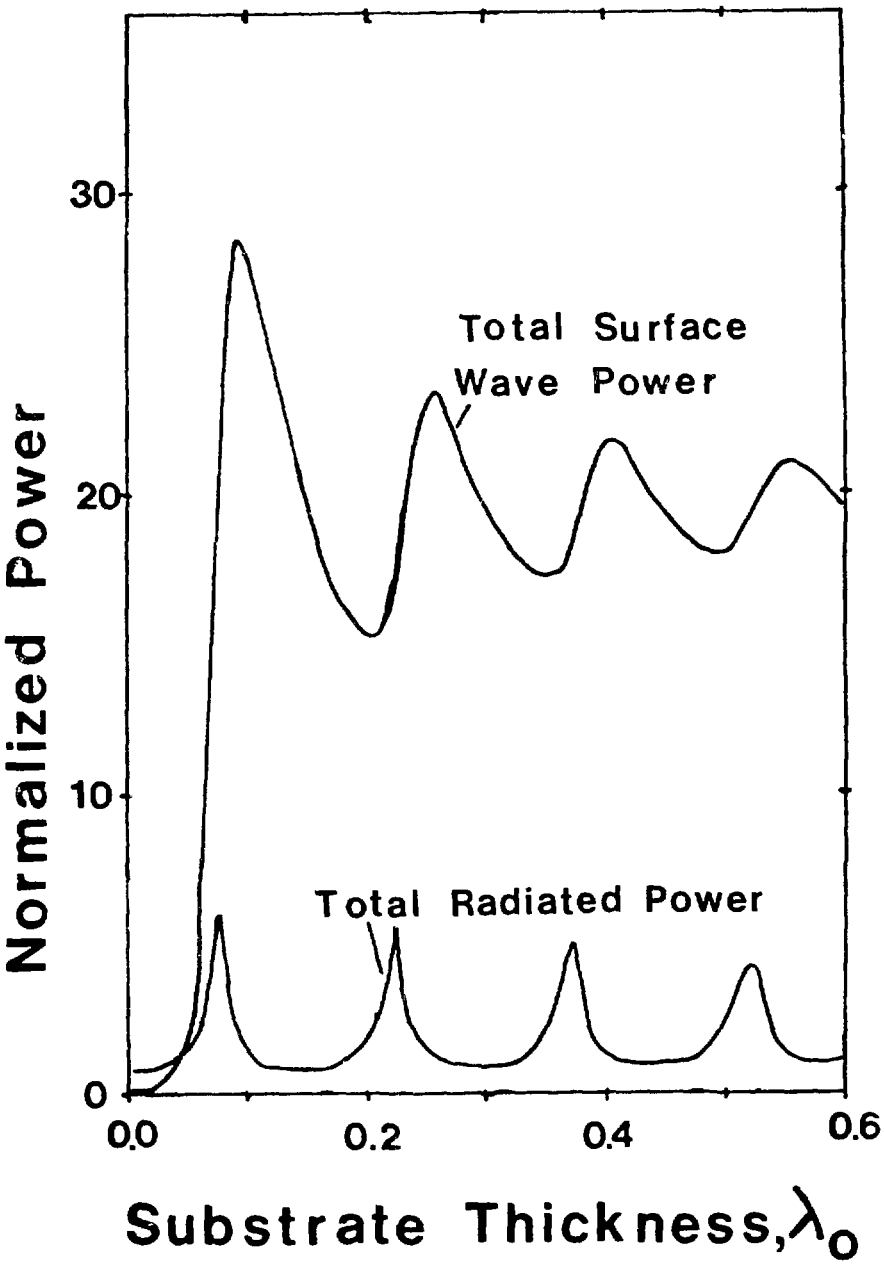

Fig. 4 Calculated distribution of power radiated by a short slot in a ground plane on a substrate with a dielectric constant of 12. Power is normalized to the power the same slot would radiate in free space. Surface waves dominate for thicknesses greater than $\lambda_o/20$.

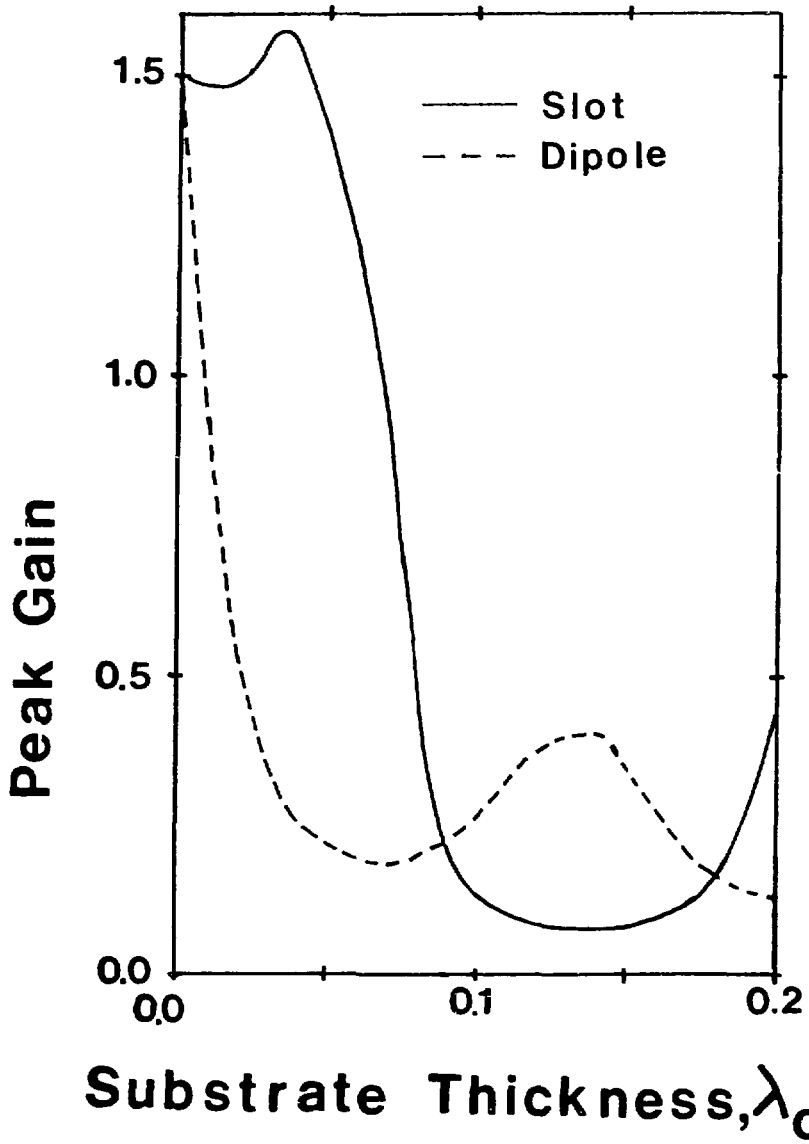

Fig. 5 Calculated peak gain of short slots and dipoles on substrates with a dielectric constant of 12. The direction for peak gain is down through the substrate. The slot gain rolls off quickly for thicknesses greater than $\lambda_o/20$. The substrate lowers the dipole gain even for thin substrates.

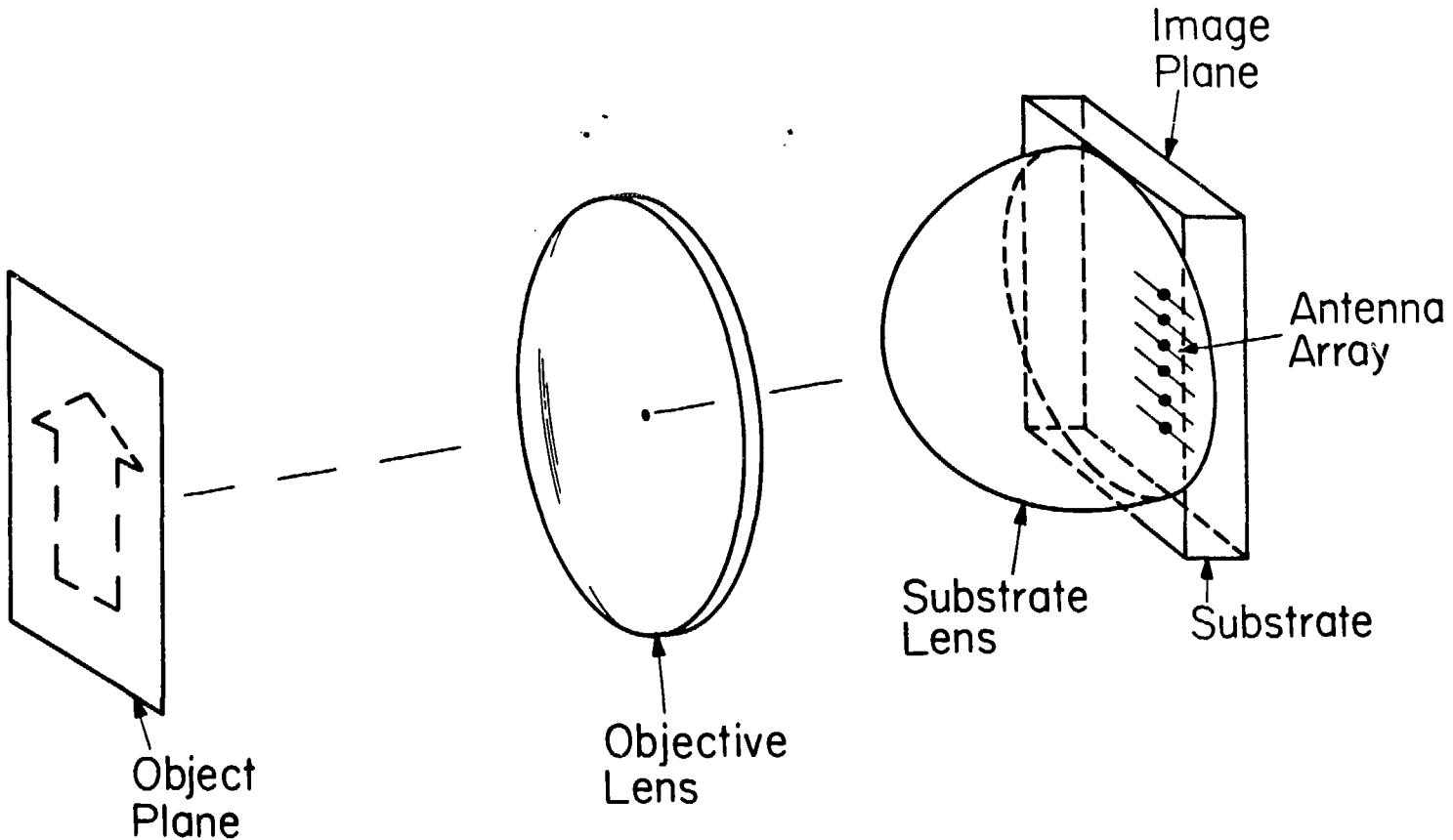

Fig. 6 Substrate-lens coupled antenna array. The substrate lens has been added to the system of Figure 1.

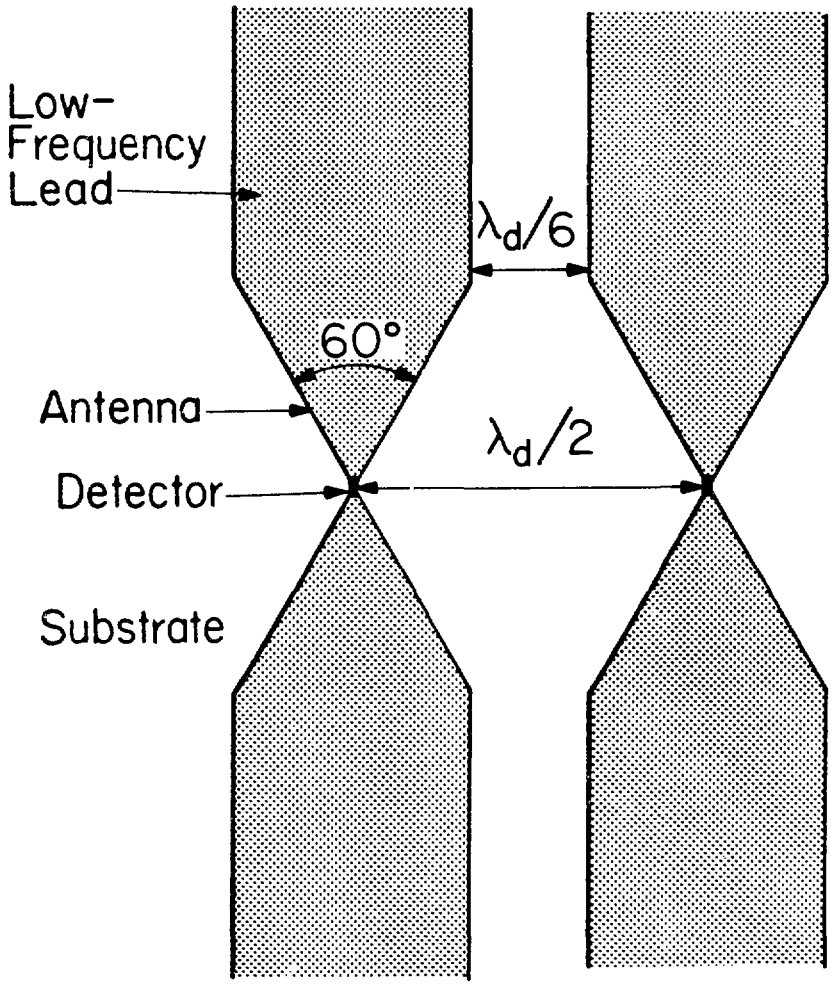

Fig. 7 Modified bow-tie for an imaging antenna array.

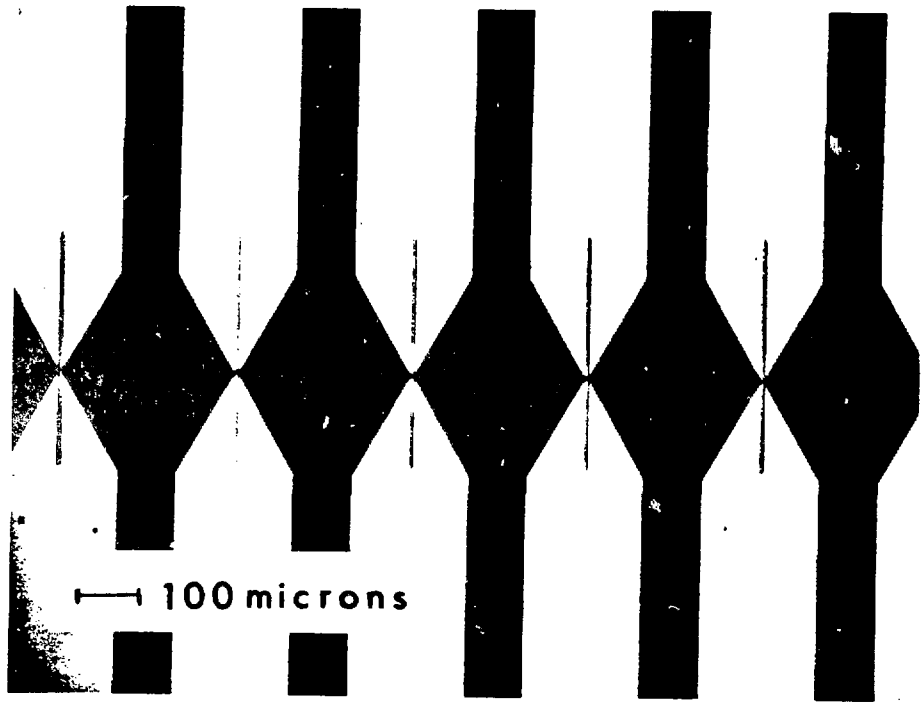

Fig. 8 Bow-tie array for a wavelength of 1.2 mm. The bow arms are evaporated silver and the substrate is fused quartz. The narrow line that crosses the gap between the arms of the bow is evaporated bismuth. The microbolometer is formed where the bismuth crosses the gap.

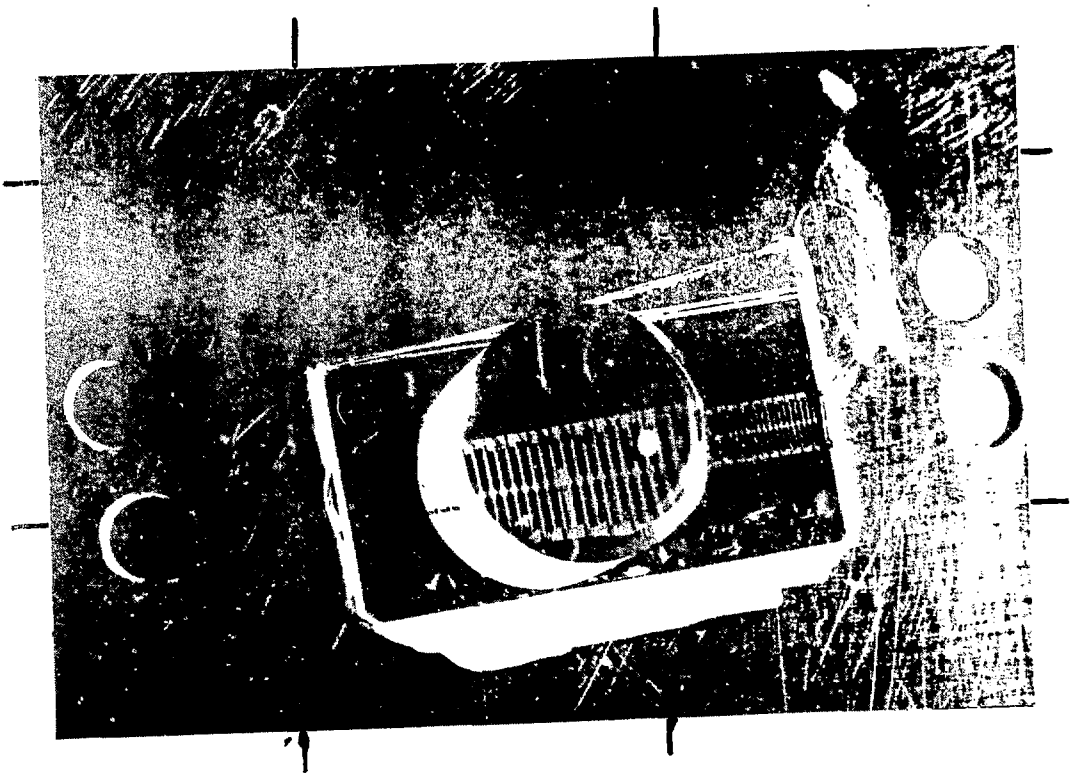

Fig. 9 Imaging array with substrate lens. The antennas are magnified by the lens.

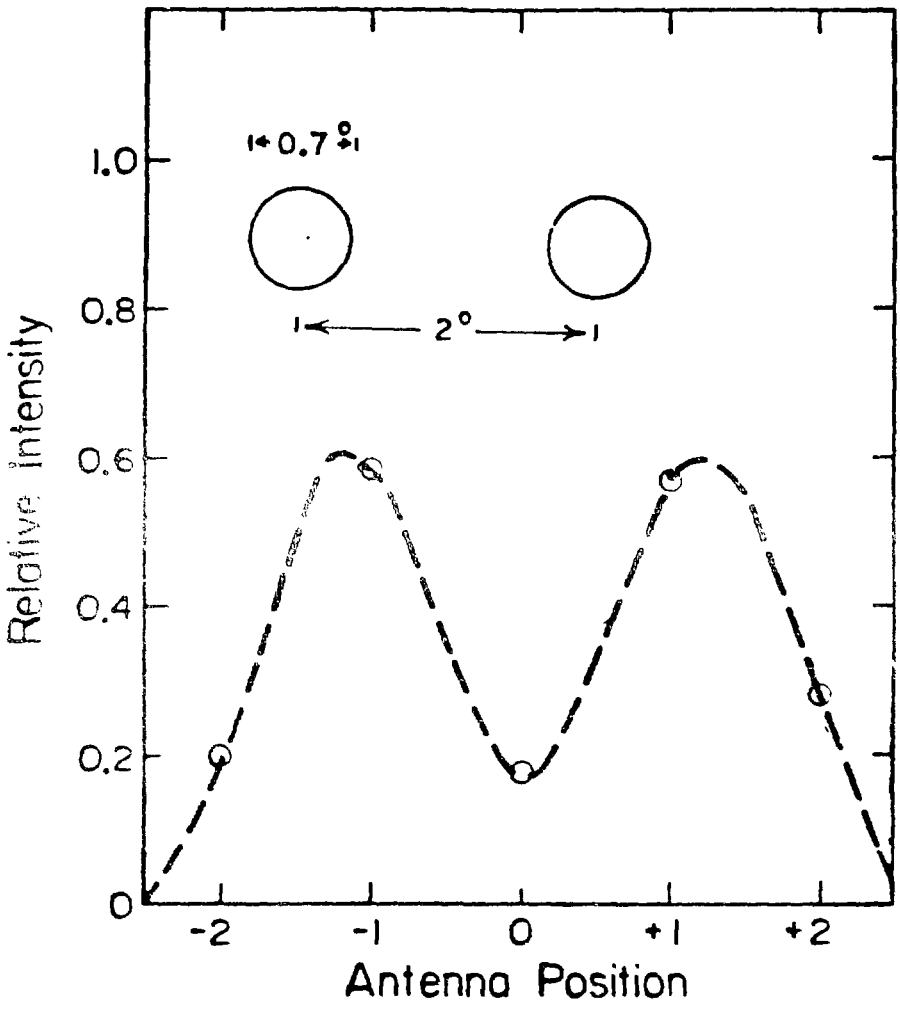

Fig. 10 Measured array images of two pinholes at 1.2 mm. The separation between the pinholes is 20% larger than the Rayleigh limit. The open circles are the observed signals. Points between the sampled values were recovered by the standard sinc-function interpolation of sampling theory (16, pp. 21-22).